DYNAMIC BEHAVIOR OF POROUS AIR BEARINGS UNDER SHOCK EXCITATION

Guilherme de Andrade Garcia [1], *Giancarlo B. Micheli* [2], *Gustavo P. Ripper* [3]

[1] Ditel-INMETRO, Duque de Caxias-RJ, Brasil, gagarcia@inmetro.gov.br
[2] Lavib-INMETRO, Duque de Caxias-RJ, Brasil, gbmicheli@inmetro.gov.br
[3] Lavib-INMETRO, Duque de Caxias-RJ, Brasil, gpripper@inmetro.gov.br

Abstract: This paper develops a mathematical model for the dynamical behavior of cylindrical air bearings when submitted to shock excitation, e.g. when support a shaft used to generate high amplitude accelerations in calibration of special purpose piezoelectric accelerometers. The results are used to evaluate a shock machine prototype.

Key words: porous air bearings, accelerometer, vibration metrology, shock excitation.

1. INTRODUCTION

Air bearings are very useful components to use in mechanical metrological instruments, due to the lowest friction coefficient that could be obtained and the very high static stiffness. However, when submitted to high impact loads, its dynamical behavior is poor and suitable measures should be taken so as not to damage the bearing surfaces. Geometrical gaps involved are very small, on the order of 5 to 10 micrometers, and even very small disturbances from the rest position can destroy the precision surfaces needed for it to work. A recent newcomer to this field is the porous air bearing, made of precision machined carbon surfaces, suitably enclosed with steel or aluminum casings. Although it solves the problem of fluid distribution over the cylindrical inner surface of the bearing, carbon is a very soft material that could easily be destroyed by mishandling.

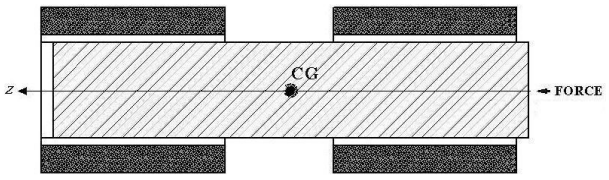

Figure 1 – Cross section view of the porous air bearings and steel anvil, to which the accelerometer is attached on the left flat surface and the shock force is applied to the right surface. CG is the center of gravity.

When using these porous air bearings for metrological shock machines to calibrate piezoelectric accelerometers, there is a pressing need to formulate a mathematical model to simulate and optimize the mechanical design. It would need the solution of the full Navier-Stokes equations applied on the flow through the porous carbon layer and along the inner cylindrical channel, to obtain the dynamic stiffness and damping coefficients. Clearly this is a daunting task in itself, and a simplified model is warranted. A drastic simplification of the physical model can be obtained using the fact that shock phenomena occur in very small periods of time, on the order of 1 millisecond or even less, and fluid cannot flow fast enough through the porous material thin channels. In this case, the fluid becomes trapped and has no time to flow, causing the air bearing film to act as a pure, non linear spring. Another simplification is the assumption of adiabatic flow, where there is no heat transfer on the shock time scale.

2. Models

2.1. Shock Machine Geometry

The shock machine under development at Lavib uses a precisely machined cylindrical stainless steel anvil that is guided by two porous air bearings, as can be seen in Figure 1. The anvil is free to slide along the axial direction *z*, but is constrained in the radial directions by the pressure differences generated by an air film flowing along the porous bearing inner surface and anvil outer surface. Two air bearings are used to support the anvil and to reduce any transversal rotation.

A mechanical impact force is generated on the right side of the anvil by the collision of an identical body, called the hammer, travelling at a speed of up to 5 m/s. The system is aligned so the force direction passes through the center of gravity (CG) of the anvil, minimizing the force moments that would cause the anvil to rotate and collide with the delicate inner air bearing carbon surface. In practice, the alignment is not perfect and it yields in an eccentric load which can cause a transversal rotation of the anvil.

Typical dimensions for this system are:

- L_a = 200 mm: anvil length;
- R_a = 20 mm: anvil radius;
- M = 2 kg: anvil mass;
- L_p = 78 mm: length of each porous bearing;
- h_0 = 5 µm: initial film gap;
- P_s = 500 kPa: supply pressure;

- P_a = 100 kPa: ambient pressure;

- τ = 1 ms: shock time duration.

2.2. Thermodynamic Model

The time dependent isothermal compressible Reynolds equation [2,3,5,6,7] is written in normalized (dimensionless) form as

$$\nabla \cdot \{H^3 \, P \, \nabla P\} = \sigma \frac{\partial (P \cdot H)}{\partial t} \tag{1}$$

where $H = h/h_0$, h is the current film gap, $P = P_s/P_a$ and

$$\sigma = 12 \left\{ \frac{\mu \, w}{P_a} \right\} \left\{ \frac{r_a}{h_0} \right\}^2 \tag{2}$$

where $w = 2\pi/\tau$ is the load frequency.

Equation 2 is known as the squeeze film number, which is a measure of the order of influence of the dynamic terms in equation 1, mainly controlled by the fluid viscosity μ.

In the limit $\sigma \rightarrow 0$ we have the quasi static case.

Due to the presence of the $\{R_a/h_0\}^2$ term in equation 2, and given R_a = 20 mm, h_0 = 5 µm, we have:

$\{R_a/h_0\}^2$ = 1,6E+7

A different situation occurs when $\sigma \rightarrow \infty$, i.e. the squeeze effect dominates the flow, since viscous flow cannot react fast enough and fluid compressibility comes into play. Equation 1 then reduces to a singular perturbation problem in the bulk of the film, away from the inlet or the outlet:

$P \cdot V$ = constant (isothermal flow) (3)

or

$P \cdot V^k$ = constant (adiabatic flow) (4)

where k is the gas specific heat ratio (1.4 for air and 1.7 for argon).

For the typical values used in our prototype we have σ = 420, for shock times τ on the order of 1 ms. This means that the air becomes trapped and has no time to flow, and the bearing film acts then as a pure, non linear spring modeled by equation 3 or 4.

The fast times involved in our shocking situation justifies the use of equation 4, that describes an adiabatic phenomena where there is no time for heat to enter or leave the system. If the fluid contracts adiabatically such that the work done is negative, then internal energy variation is positive and the fluid temperature increases.

As delineated by Richer and Hurmuzlu in [4], the system could be modeled also as an intermediate situation between purely isothermal and purely adiabatic. This can be done simply by assuming the coefficient k has an intermediate value between 1 and k, what effectively reflects in transforming equation 3 into equation 4.

The considerations stated above provides the support the use of a much simpler mathematical approach when dealing with situations of shock phenomena, applying equation 4 together with the geometry shown in figure 1.

2.3. Initial and Boundary Conditions for Air Flow and Speed

An important initial step is to discover if our assumptions about flow speed and pressure distribution in the air gap are true in the case of cylindrical porous air bearings. The scientific literature yielded no data, so it was necessary to adapt a 1D model [1] developed for planar porous bearings to produce the necessary information for cylindrical ones.

A computational code has been developed in MatLab environment. The processing time proved to be very short and the results obtained agreed well with more complex 3D formulations [3].

Axially pressure distribution and air flow speed obtained with the use of this code could be seen in figures 2 and 3, respectively, where distance starts at the air bearing center and extends symmetrically to the borders.

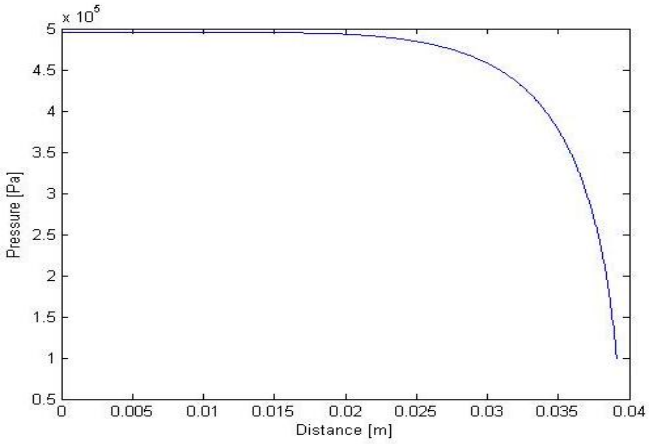

Figure 2 – Axially pressure distribution from center to end of the air bearing, for a supply pressure of 500 kPa and h_0 = 5 µm.

Our main hypothesis is that we have a situation where air cannot flow fast enough inside the air gap, but we can see in figure 3 that on the outer border we have a high velocity region where flow speed reaches almost 30 m/s. Also in figure 2 we can notice that pressure drops very fast due to this flow acceleration, falling from 500 kPa to 100 kPa in a short distance.

Air temperature information can also be extracted from the simulation and is constant along this path, changing less than 0.4 °C mainly around the edges.

Due to these characteristics, it was chosen to exclude the edge regions from calculations in the model, so as not to overestimate the forces involved. To quantify the extension of this region we estimate how much the fluid would move during the shock time duration τ:

$$v\left(z-\frac{L_p}{2}\right)\cdot\tau = z-\frac{L_p}{2} \tag{5}$$

After solving equation 5 numerically, the following results were obtained: z_{lim} = 35 mm and $v(z_{lim})$ = 3,5 m/s.

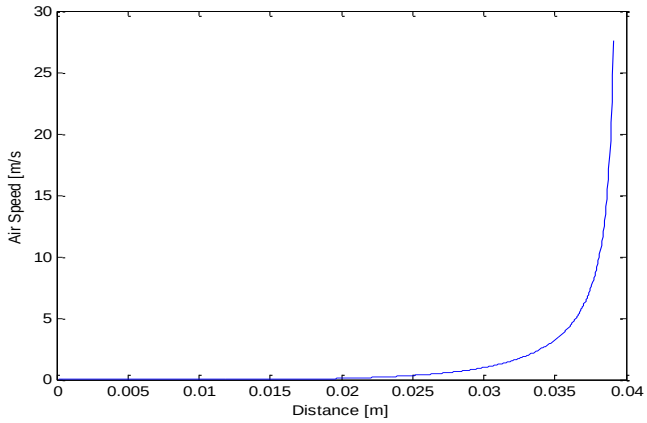

Figure 3 – Air speed versus axial distance from center to end of the air bearing, for a supply pressure of 500 kPa and h_0 = 5 µm.

Another characteristic to bear in mind is one of a geometrical nature. In a catastrophic limiting situation where the hard outer anvil surface touch the soft inner carbon surface, the volume of a discretized geometric element just on the edge of the air bearing will tend to zero. Blind application of equation 4 will then produce infinite pressure and infinite force, what is clearly not a realistic physical situation that must be excluded from our algorithm.

2.4. Geometrical Modeling and Equations of Motion

Applying equation 4 to a differential volume element dV we obtain

$$P_0\, dV_0^k = P_i\, dV_i^k \tag{6}$$

The air gap volume between the anvil and porous bearing was discretized as a section of the wedge centered along the axial symmetry axis z.

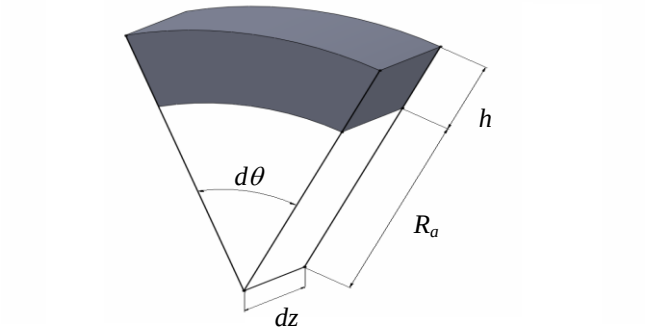

Figure 4 – Wedge shape discretized volume dV, where $h = h(z,\theta)$, dz is the differential distance along the anvil central axis, $d\theta$ is the angular differential element.

As can be seen in figure 4 our differential volume element could then be obtained as

$$dV_i = h(z,\theta)\cdot\left\{R_a+\frac{h(z,\theta)}{2}\right\}\cdot d\theta\cdot dz \tag{7}$$

Further manipulation results in

$$P_i(z,\theta,\alpha) = \frac{P_0\, h_0^k\,\{R_a+h_0/2\}}{h^k(z,\theta,\alpha)\,\{R_a+h(z,\theta,\alpha)/2\}} \tag{8}$$

The simplifications outlined allow us to build a set of first order differential equations, including the non-linear spring behavior and the dynamical equations of motion [3]. The steel anvil was assumed completely rigid solid body, and any deformation was ignored in this analysis.

$$\frac{d\,z(t)}{dt} = v(t) \tag{9}$$

$$\frac{d\,v(t)}{dt} = -\frac{F(t)}{M} \tag{10}$$

→ $z(t)$ is the longitudinal displacement

→ $v(t)$ is the longitudinal velocity

The applied shock force $F(t)$ was modeled with a half-sine shape, applied at a distance Δx in mm away from the cylindrical symmetry center line.

$$F(t) = \frac{\pi}{2}\left\{\frac{M\,V_i}{\tau}\right\}\sin\left(\frac{\pi\,t_i}{\tau}\right) \tag{11}$$

where V_i is the final velocity imparted to the anvil.

$$\frac{d\,\alpha(t)}{dt} = \beta(t) \tag{12}$$

$$\frac{d\,\beta(t)}{dt} = \frac{1}{I_x}\left\{F(t)\cdot dx + 2\cdot\zeta\cdot\beta(t) - b\cdot K(i,j)\right\} \tag{13}$$

→ $\alpha(t)$ is the angular displacement in the plane containing the CG and the force applied, centered in the CG

→ $\beta(t)$ is the angular velocity

→ I_x is the principal moment of inertia of the steel anvil taken along the axial direction, and calculated as $\{ML^2/12\}$

→ ζ is the damping coefficient,

The air gap volume around the steel anvil was discretized and forces calculated as discrete summations over these volume elements.

$$K(i,j) = \sum_{i=1}^{NZ-1}\sum_{j=1}^{NT-1}\frac{\{BZ_i + BT_j\}}{\{f(i,j)\cdot\{R_a+f(i,j)\}\}^k} \tag{14}$$

$$f(i,j) = h_0 - a(t)\cdot BZ_i\cdot BT_j \tag{15}$$

$$b = 2\cdot 2\cdot p_{\max}\cdot h_0^k\cdot\{R_a+h_0\}^{k+1}\cdot ddt\cdot ddz \tag{16}$$

The arm momentum, that is the distance from the center of gravity CG where the force arising from pressure differences is applied, is given by

$$BZ_{iz} = z_0 + edge + (iz+1/2)\cdot ddz \tag{17}$$

A short band around the cylinder ends (~4 mm) was not considered in the calculations, since we assume that air flow

speed is high and compression effects are small in this area, as already discussed.

The discretized angles along the half circle where the discrete force integral are calculated is given by

$$BT_{it} = \cos[(it + 1/2) \cdot ddt] \tag{18}$$

$$ddz = \frac{L_a - 2 \cdot edge}{NZ + 1} \tag{19}$$

$$ddt = \frac{\pi}{NT + 1} \tag{20}$$

→ NZ is the number of discrete elements dz along the air bearing length

→ NT is the number of angular discrete elements related to the angular differential element $d\theta$ in figure 4

Equations 13 to 19 derived from several symmetry properties arising from figure 1.

2.5. Dynamical Behavior

In figure 4 we can see the resulting dynamical displacement of the steel anvil extremity around the central rest position. The anvil tip is the position that suffers the most extreme displacement due to the rotational motion imparted by the large moments applied. We used actual physical parameters from the experimental setup, assuming one millisecond shock duration and a rather high 1 mm eccentric distance from the cylindrical axis of symmetry.

Porous carbon air bearing surfaces are located at the bottom (h = 0) and top (h = 10 µm) of the graph. Solid line shows the upper anvil tip edge, and the dashed the lower anvil tip edge.

In figure 5 we could see at 0.5 ms the shock end and the beginning of the free oscillatory movement. The damping coefficient was set at a low value and the oscillation continues for a time much longer than the shock duration.

The oscillatory movement comes from the air spring action transferring energy to the anvil, which appears as a transversal acceleration measured by the piezoelectric accelerometer. Even assuming a very high off center shock force, the simulation results predicts small oscillatory displacements that did not impact the inner porous carbon surfaces located at the bottom (h = 0) and top (h = 10 µm) of the graph.

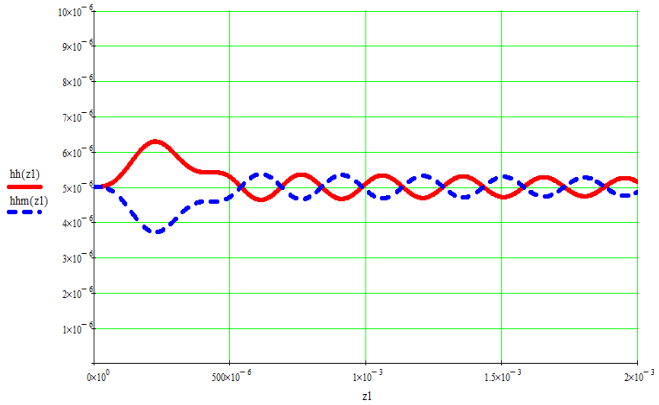

Figure 5 – Relative position of the anvil edges inside the gap area (from rest position at 5 µm), for an applied 0.5 ms shock duration. Bottom axis is time in seconds.

In figure 6 we can see the shock signals, where the steel anvil starts from rest and reach the final velocity (solid line) after the end of the shock. The dashed line shows the longitudinal displacement, which grows unbounded until the anvil reaches an obstacle.

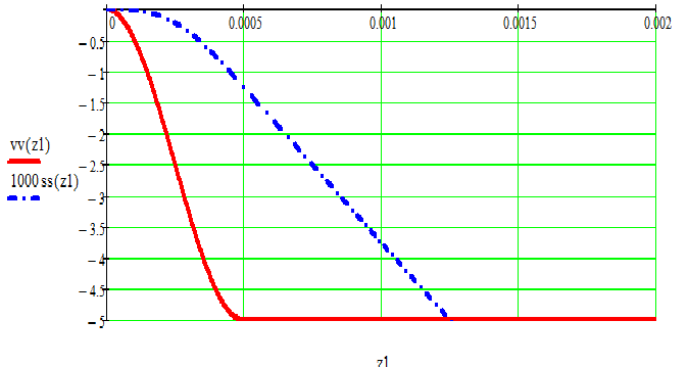

Figure 6 – Steel anvil axial velocity (solid line) and axial displacement (dashed line). Bottom axis is time in seconds.

In figure 7 we can analyze the condition where the damping coefficient is higher, and the oscillatory movements decays very fast.

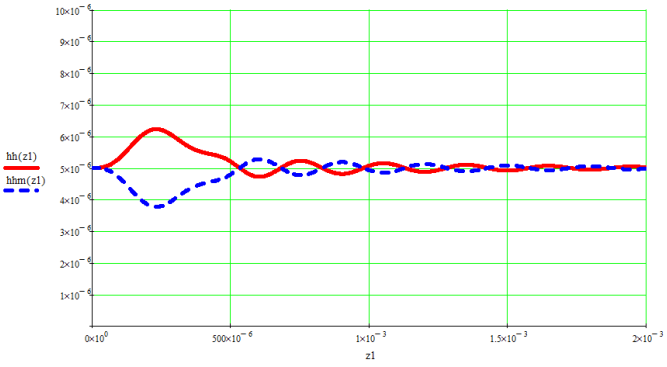

Figure 7 – Relative position of the anvil edges inside the gap area (from rest position at 5 µm), for an applied 0.5 ms shock duration. In this graph the damping was set at a higher value, and we could see the very fast attenuation of the oscillations. Bottom axis is time in seconds.

Another interesting possibility is the use of the degree of freedom proportional to the exponent k in equation 4. Changing the gas from clean dry air to argon, the exponent will change from k = 1.4 to k = 1.7 and the corresponding displacement graph can be seen in figure 8. We can notice the lower maximum displacement that is a definite advantage in our situation, so that it could prevent damage to the carbon air bearing surface. With care you could notice also that the subsequent oscillatory movement has slightly higher amplitude.

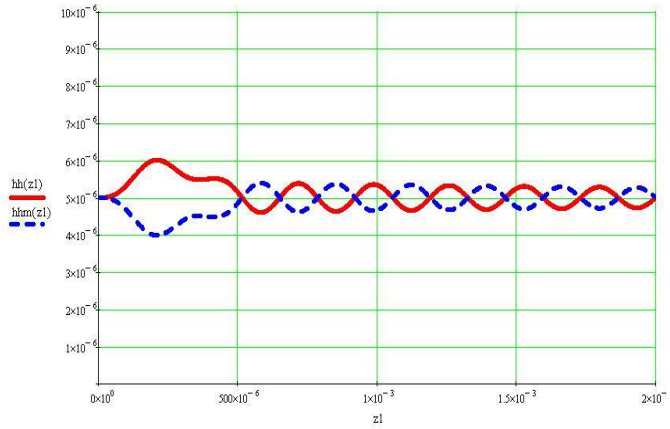

Figure 8 – Relative position of the anvil edges inside the gap area (from rest position at 5 µm), for an applied 0.5 ms shock duration. Coefficient k = 1.7 (adiabatic case with argon gas). Bottom axis is time in seconds.

Another possibility is the investigation of the hypothesis regarding our choice between equation 3 or 4, in section 2.2. As stated before, reference [4] shows that you can model an intermediate situation between purely isothermal to purely adiabatic by changing the coefficient k from 1 to k. If we set k = 1.0 we have the isothermal case, as can be seen in figure 9. A notable characteristic of this situation is that the maximum displacement is two times higher than before, implying that the chance of damage to the carbon inner surface is much higher than in the other situation. Also we can notice that the oscillations are much lower in amplitude, meaning that the air spring has a much lower effect.

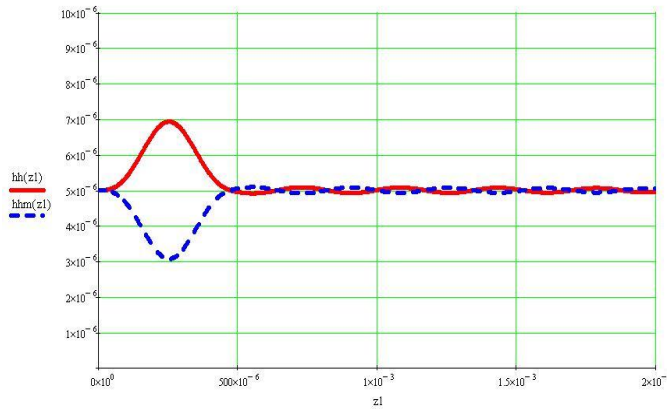

Figure 9 – Relative position of the anvil edges inside the gap area (from rest position at 5 µm), for an applied 0.5 ms shock duration. Coefficient k = 1.0 (isothermal case). Bottom axis is time in seconds.

3. CONCLUSION

The model presented in this paper retrieves some essential features that occur during the shock phenomena, including maximum anvil excursion and oscillation frequency. The characteristics of the operation as an isothermal or adiabatic system were investigated, showing that the use of argon as a gas of choice will be beneficial. Using the chosen geometrical parameters we can see that the anvil experiences a small oscillatory movement around the axis of symmetry, and did not hit the air bearing inner surface made of soft porous carbon. Further analysis should be done to compare our predictions to experimental data obtained from the prototype shock machine.

A numerical code was adapted from the literature to allow the determination of the initial pressure and air flow conditions along the air gap.

AKNOWLEDMENTS

The authors would like to acknowledge the very helpful suggestions from Dr. Alexander Slocum-MIT.

REFERENCES

[1] A design model for circular porous air bearings using the 1D generalized flow method, Jean-Sebastien Plante, John Vogan, Tarek El-Aguizy, Alexander H. Slocum, Precision Engineering 29 (2005), 336–346.

[2] Design of optimized opposed slider air bearings for high speed recording on a metal foil disk, James White, ASME Journal of Tribology, Volume 128, Issue 2, 327, 2006.

[3] Static study of the porous bearings by the simplified finite element analysis, Yong Tian, 203-209, Wear 218 (1998).

[4] A High Performance Pneumatic Force Actuator System–Part 1: Nonlinear Mathematical Model, E. Richer, Y. Hurmuzlu, ASME Journal of Dynamic Systems Measurements and Control, 122-3, pp 416-425, 2000.

[5] Studying fluid squeeze characteristics for aerostatic journal bearing, G. M. Abdel-Rahman, Physica B 403 (2008), pp 2390-2393.

[6] Comparison between externally pressurized gas thrust bearings with different orifice and porous feeding systems, M. Fourka, M. Bonis, Wear 210 (1997), pp 311-317.

[7] Dynamic tilt characteristics of aerostatic rectangular double-pad thrust bearings with compound restrictors, S. Yoshimoto, J. Tamura, T. Nakamura, Tribology International 32 (1999), pp 731–738.